

PROCEEDINGS OF SPIE

SPIDigitalLibrary.org/conference-proceedings-of-spie

Two-photon laser lithography in optical metrology

Julian Hering, Matthias Eifler, Linda Hofherr, Christiane Ziegler, Jörg Seewig, et al.

Julian Hering, Matthias Eifler, Linda Hofherr, Christiane Ziegler, Jörg Seewig, Georg von Freymann, "Two-photon laser lithography in optical metrology," Proc. SPIE 10544, Advanced Fabrication Technologies for Micro/Nano Optics and Photonics XI, 1054412 (22 February 2018); doi: 10.1117/12.2289900

SPIE.

Event: SPIE OPTO, 2018, San Francisco, California, United States

Two-photon laser lithography in optical metrology

Julian Hering^{*a}, Matthias Eifler^b, Linda Hofherr^a, Christiane Ziegler^a, Jörg Seewig^b, and Georg von Freymann^{a,c}

^aPhysics department and state research center OPTIMAS, University of Kaiserslautern, 67663 Kaiserslautern, Germany;

^bInstitute for Measurement and Sensor Technology MTS, University of Kaiserslautern, 67663 Kaiserslautern, Germany;

^cFraunhofer Institute for Industrial Mathematics ITWM, 67663 Kaiserslautern, Germany

ABSTRACT

Two-photon laser lithography has become one of the most promising additive manufacturing techniques on the micron scale and is applied, e.g., in fields of micro-optics and -robotics as well as optical and mechanical metamaterials. Here, we report on the feasibility, limits and general benefits of this method to fabricate material measures for the calibration of industrial optical topography measuring devices. Since calibration procedures are essential in the scientific and industrial application of those measuring instruments, appropriate material measures are highly required. In contrast to traditional manufacturing technologies, we show that two-photon laser lithography allows a highly resolved fabrication of multiple, almost arbitrary standardized calibration geometries on a micron length scale. Hereby, all structures are fabricated on only one single substrate, therefore enabling a mapping of a broad range of metrological characteristics for topography characterization. The most required calibration geometries are manufactured and analyzed regarding their aging behavior, their quality improvement by a post-UV development and the resolution limits within the manufacturing as well as the calibration process. Thus, the general industrial and scientific relevance of manufacturing material measures with two-photon laser lithography is demonstrated.

Keywords: direct laser writing, two-photon polymerization, additive manufacturing, calibration, artefacts, material measures, areal/profile surface metrology, ISO standardization, topography measuring instruments

1. INTRODUCTION

For the acquisition of reliable topography data in science and industry achieved by an accurate use of optical topography measuring instruments, all limits of the respective devices must be known and have to be considered. To guarantee traceability and comparability of varying measuring devices worldwide, an internationally standardized calibration is indispensable, especially for the enormously growing field of areal surface topography measurement [1,2,3]. To regulate this demand on standardization, first parts of the standard ISO 25178 [4] have been published since 2010 and publishing of the remaining open topics is still work in progress.

The most common calibration parameters to be characterized are the lateral resolution limit, noise and residual flatness, linearity, perpendicularity and amplification coefficient of the lateral axis, as well as linearity and amplification coefficient of the height axes, which can be determined by the approach of Giusca et al. [5,6,7]. Besides, the so-called ‘small scale fidelity’ was introduced in 2014 [8] as another characteristic to identify the resolution of the measuring device. Exemplarily, Figure 1 shows two important material measures of the aforementioned ISO 25178 standard (part 70) and the corresponding importance of a correct calibration: the areal flatness standard (AFL-type) for calibrating the residual flatness and the instrument noise (Figure 1 a) as well as an (areal) lateral cross-grating (ACG-type) for the calibration of the linearity, the amplification coefficient and the perpendicularity of the device’s x - and y -axis (Figure 1 b). By determining and considering those measuring instrument’s properties due to calibration procedures and subsequent adjustments, the obtained measurement data can be acquired in a proper way and it can be ensured that the true surfaces are imaged correctly and reliably within a defined uncertainty range.

*hering@physik.uni-kl.de

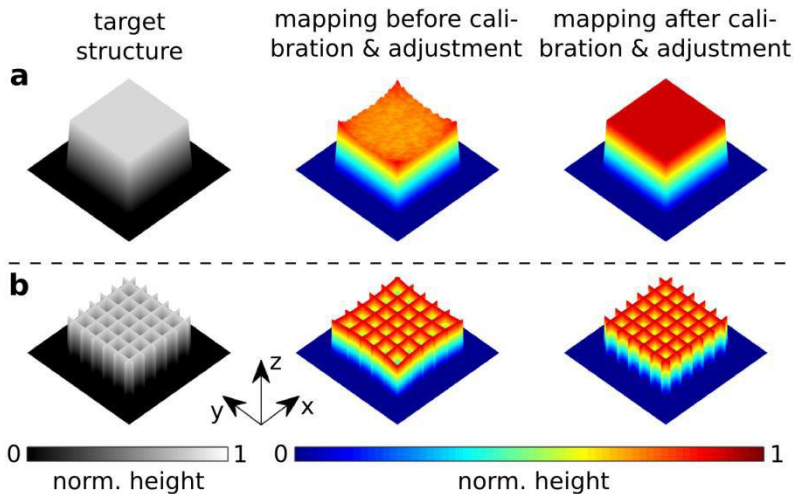


Figure 1. Schematic comparison between a calibrated & adjusted and a not calibrated & adjusted topography measurement (simulated). Two common calibration measures are shown: an AFL-type measure for calibrating noise and residual flatness (a) as well as an ACG-type measure for the calibration of the lateral axis' perpendicularity, amplification coefficient and linearity (b).

Up to date, varieties of material measures are used for the calibration of the previously described metrological characteristics. A first minimized set of five different types of samples was introduced by the so-called 'NPL BentoBox' in 2013 by Leach et al. [9]. However, one single sample featuring all of the required and desired calibration geometries for an easy and particularly time-saving calibration procedure is still missing. This is due to the manufacturing process of the material measures which require varying geometry- and scale-dependent fabrication techniques.

For a flexible manufacturing of structures on different length scales, additive manufacturing, especially two-photon laser lithography (alias direct laser writing, DLW) [10-12] is very promising. This fabrication method is already established for generating freeform three-dimensional structures ranging from the centimeter scale [13] down to sub-micron feature sizes and resolution [14,15]. Research fields as diverse as photonic crystals [16], aperiodic structures [17], micro-optics [18,19] and -robotics [20], cell-templates [21,22], metamaterials [23,24] as well as first steps in calibration geometries for optical metrology [25-27] are addressed by DLW. For further improvement of the structure-quality regarding resolution and fabrication-parallelization, aberration correction approaches [28,29] and the generation of application-tailored point spread functions (PSF) [30,31] are of great advantage. Furthermore, DLW is not necessarily restricted to the optical resolution limit [32] of the excitation laser any longer: inspired by the work of Nobel Prize laureate Stefan Hell [33,34], the principles of stimulated emission depletion (STED) can be transferred to lithography as well to improve the geometries' resolution, mechanical stability and general quality [35,36].

Here, we demonstrate that DLW is also the technique of choice for manufacturing material measures.

2. MATERIALS AND METHODS

The detailed principles of the DLW process are well known and can be found elsewhere [10,12]. In a nutshell: a femto-second pulsed laser beam (central wavelength $\lambda = 780$ nm) is focused by a high numerical aperture objective (NA 1.4, 63x) into a negative-tone photoresist. Here, the incorporated energy is absorbed via two-photon absorption, leading to a generation of radicals and thus, a polymerization within the very focal volume. Hence, a relative movement of laser-focus and photoresist results in a three-dimensional structure which can be revealed by a subsequent development step (PGMEA and Isopropanol are used as solvents here). Inspired by the work of Oakdale et al. [37], an additional post-UV development process is used to improve the stability of the fabricated structures. We compare both fabrication approaches with regard to the different metrological characteristics of the aforementioned most required material measures.

Two different laser lithography systems are utilized: a 'Photonic Professional GT' (*Nanoscribe GmbH*) combined with the commercial photoresist 'IP-S' (*Nanoscribe GmbH*) for low shrinkage behavior and high conformity of target- and actual-structure is used. On the other hand, a self-built DLW system including a spatial light modulator (SLM, 'X10468-01', *Hamamatsu Photonics K.K.*) for aberration correction and the opportunity of switching to 'STED-inspired DLW' is used for fabricating high-resolution structures. Here, we use the commercial photoresist 'IPL-780' (*Nanoscribe GmbH*),

since it is specified for highest resolution. Additionally, its photo-initiators can be depleted by a focused continuous-wave laser beam with a central wavelength at $\lambda = 532$ nm.

The respective calibration measures are realized as stereo-lithography (.stl) data types and translated into x , y and z coordinates with the aid of the software ‘Describe’ (*Nanoscribe GmbH*) for the relative movement of the laser-focus. For all geometries, a galvanometer mirror scan speed of 20,000 $\mu\text{m/s}$ is used.

As most of the optical topography measurement instruments cannot measure polymeric calibration surfaces reliably due to the high transparency to visible light, a reflective coating of the geometries is indispensable. Since gold (Au) serves as standard coating material for optical applications, it is investigated first. Due to the weak bonding between gold and the (glass) substrate, chromium is usually used as adhesion-promoting agent, just as in this work. Therefore, chromium (Cr) is analyzed as coating material as well. Both metals are characterized by sufficient optical reflectivities (Au: ~70%, Cr: ~55% for $\lambda = 532$ nm at an angle of incidence of 0° [38]), as well as sufficient high Vickers hardnesses (Au: ~200 MPa, Cr: ~1000 MPa [39]), enhancing the geometries’ mechanical stability. For both materials, a ‘UNIVEX 450 C’ (*Oerlikon AG*) sputter device is used to grow 30 nm thin metal layers. Apart from that, iridium is characterized by an even higher Vickers hardness of about 2000 MPa [39] and possesses a similar optical reflectivity (~70% [40]). Therefore, it is also investigated as coating material and sputtered by the high vacuum coating device ‘Leica EM ACE600’ (*Leica Microsystems GmbH*).

To investigate the industrial and practical relevance of the fabricated calibration samples, their aging behavior and the influence of the varying coatings on this behavior are analyzed. Since aging is a time-dependent process [41], the samples are stored within a ‘VT 4010’ climate chamber (*Vötsch Industrietechnik GmbH*) at 80°C for up to 19 days in order to induce an accelerated artificial aging. In addition, drying agents are deployed into the chamber in order to ensure dry air conditions. Previously, it has been shown that this method is suitable for the description of aging-effects for measures fabricated with ultra-precision cutting [42] and, thus, should be used to investigate the aging behavior of direct laser written geometries as well.

For a first qualitative analysis of the fabricated calibration measures, a ‘Hitachi SU8000’ scanning electron microscope (SEM) (*Hitachi K.K.*) is used. By comparing different manufactured geometries, the most promising fabrication parameters are identified and used for any following investigations. To assess their practical and industrial applicability and to observe their aging behavior, a ‘ μSurf ’ confocal microscope (CM) (*NanoFocus AG*) is used. Considering the different objective magnifications, all geometries are scaled into footprints of $100 \times 100 \mu\text{m}^2$, $200 \times 200 \mu\text{m}^2$, $400 \times 400 \mu\text{m}^2$ and $800 \times 800 \mu\text{m}^2$, while keeping their heights constant. Structures greater than $200 \times 200 \mu\text{m}^2$ are stitched together from fields of maximal $120 \times 120 \mu\text{m}^2$ to reduce the influence of distortion and vignetting during the laser scanning process. In the following, we only show the results for the first footprint for clarity. For identifying the detailed geometry-dependent resolution limits of the fabrication procedure and to evaluate the final quality of the calibration geometries, a ‘JPK NanoWizard 3’ scanning force microscope (SFM) (*JPK Instruments AG*) is used, utilizing ‘SNL-10C’ cantilevers

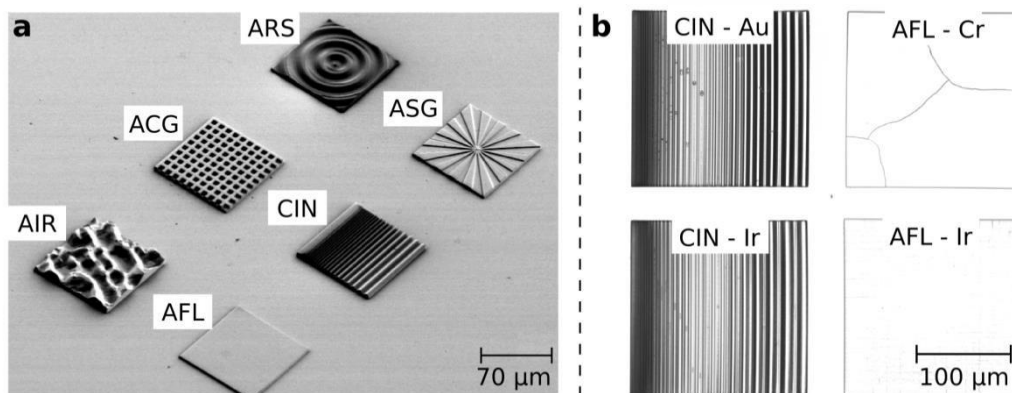


Figure 2. Material measures. SEM image of the so-called ‘universal-sample’ ($100 \times 100 \mu\text{m}^2$ structures part), containing the six calibration geometries, which allow the calibration of the most relevant metrological characteristics (a). Light microscopic images of the respective gold, chromium and iridium sputtered measures (b). The gold layer shows several micro-crystalline ‘crumbs’, the chromium layer shows cracks, whereas the iridium layer demonstrates the best quality.

(spring constant 0.12 N/m, resonance frequency 40 kHz, setpoint 5.5 nN, *Bruker corp.*) in contact-mode, as well as ‘Tap150DLC’ cantilevers (force constant 5 N/m, resonance frequency 150 kHz, setpoint 30.0 nN, *BudgetSensors*) in quantitative imaging mode. Here, 40 x 40 μm^2 structures with decreased height amplitudes of 1 μm (peak-to-valley) are fabricated. Due to the SFM’s high resolution, these dimensions are definitely sufficient for the intended investigation.

3. RESULTS AND DISCUSSION

3.1 Durability of the calibration geometries – aging

The aforementioned most common metrological characteristics can be determined and calibrated by the six geometries shown in Figure 2 a. Thanks to direct laser writing, all of these geometries can be manufactured onto one single sample, leading to enormous time savings during the subsequent calibration procedures of optical measurement devices: there is no need of installing and removing an amount of different samples any longer within a holistic calibration of an industrial measuring instrument.

After a first light microscopic analysis of the different coating materials, gold and chromium are determined to be not well suited. Due to the micro-crystalline growth of the gold layer, ‘crumbs’ are found within the valleys of the chirp-type measure (CIN), as imaged in Figure 2 b, left-hand side. Since chromium grows under very high tension, the polymeric network underneath the coating surface strongly expands when the structure is released to atmospheric conditions after the sputtering process, resulting in irregular cracks, especially for larger polymerized volumes (see Figure 2 b, right-hand side). In contrast, the iridium surface does not show any unintended distortions (see Figure 2 b, bottom). As the material measures should be suitable for a calibration of tactile measuring instruments as well, the higher hardness of iridium is another great benefit. Therefore, iridium is determined as the coating material of choice.

Hence, the green curves in Figure 3 show the time-dependent aging behavior of the iridium-coated calibration geometries, exemplary for the 100 x 100 μm^2 AFL-type (Figure 3 a, CAD-illustration on the left-hand side) and AIR-type (Figure 3 b, CAD-illustration on the left-hand side) measure. Here, the arithmetic areal mean roughness $S_a = \frac{1}{A} \iint_A |Z(x,y)| dx dy$ is depicted for instance. It can be observed that during the first days, the roughness values vary irregularly above the target value and stabilize after a period of time (note the substantially smaller y-scale in Fig. 3a). This can be explained by the temperature-dependent delayed polymerization of the photoresist. After the fabrication process, there are still several radicals and not cross-linked polymeric parts left which can be associated by temperature annealing. This leads to a smoothening effect of the respective surfaces and thus, to gradually approaching the target values. The red curves in Figure 3 show the respective results for the above mentioned additional post-UV exposure of the fabricated geometries. The initial irregular variations of S_a are suppressed and the measured values are nearly constant over the complete observed aging time. In addition, these values are significantly closer to the target value. Under UV exposure, the additional photo-initiator molecules within the solvent (Isopropanol + Irgacure 654) polymerize unreacted acrylate groups. As a result, the cross-linking density is increased in such a way that the surfaces smooth out, leading to an instant reduction of S_a . Since this procedure is much faster than a several-days-storage within a climate cham-

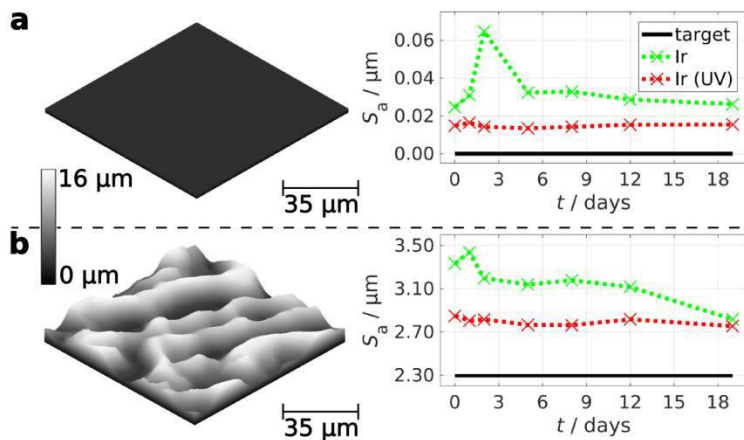


Figure 3. Aging behavior of the calibration geometries. The area roughness parameter S_a (acquired by a CM, 100x objective) is shown over a total time of 19 days for the AFL-type (a) and the AIR-type (b) material measures (CAD-data on the left-hand side). A post-UV exposure noticeably improves and stabilizes the roughness parameter. Note the substantially smaller y-scale in (a).

ber, the post-UV curing process is established for all following experiments.

Nevertheless, the predefined roughness values cannot be reached because of various reasons: during the fabrication procedure, there are fluctuations of the galvanometer mirror-, piezo- and stage-positions. Besides, influences of vignetting and aberrations have to be mentioned. As a further reason, the sputtered coating layers do not grow in a perfect homogeneous way, leading to additional height variations. Furthermore, the measuring confocal microscope is characterized by a specific measurement uncertainty and certain light-matter interactions add up to the finally observed deviations from the target values. Most of these aspects are caused by technical reasons and cannot be compensated. Using the aforementioned SLM(s) provides the possibility to correct aberrations present in the experimental setup. The resulting improvements are discussed within the following section.

3.2 Resolution limits for fabricating calibration geometries – aberration correction and STED

To determine the lateral resolution capabilities of optical topography measuring instruments, two of the already mentioned calibration geometries are useful: the ASG-type (Areal Star-Shaped Grooves or ‘Siemens-Star’, Figure 4 a, CAD-illustration on the left-hand side) and the chirped measure (CIN-type, Figure 4 b, CAD-illustration on the left-hand side) which are both examined with a footprint of $40 \times 40 \mu\text{m}^2$ and a peak-to-valley height amplitude of $1 \mu\text{m}$. The other way round, these geometries can also be utilized to determine the resolution limit of the manufacturing process, when a high-resolution measuring device like a scanning-force-microscope (SFM) is used for the characterization. For the ASG-type, the SFM-acquired height profiles through the center of two opposing sunken and two opposing elevated petals are extracted from the measured 3D-topography. The difference between these two profiles is defined as instrument response profile (IRP), whose lateral scale is multiplied by π/n , where n is the number of the petals (here: $n = 16$). The full width at half maximum (FWHM) of the resulting central height-peak represents the ISO-based lateral period limit d and serves as parameter for the lateral resolution of the manufacturing process [7].

For the CIN-type measure, the small scale fidelity limit (ssf) is used as resolution-describing characteristic [8,43]. Here, the locally decreasing wavelength-topography (in the examined case: $5.20 \mu\text{m}$, $4.57 \mu\text{m}$, $4.02 \mu\text{m}$, $3.54 \mu\text{m}$, $3.11 \mu\text{m}$, $2.74 \mu\text{m}$, $2.41 \mu\text{m}$, $2.12 \mu\text{m}$, $1.86 \mu\text{m}$, $1.64 \mu\text{m}$, $1.44 \mu\text{m}$, $1.27 \mu\text{m}$, $1.12 \mu\text{m}$, $0.98 \mu\text{m}$, $0.86 \mu\text{m}$, $0.76 \mu\text{m}$, $0.67 \mu\text{m}$, $0.59 \mu\text{m}$, $0.52 \mu\text{m}$, $0.46 \mu\text{m}$, $0.40 \mu\text{m}$) of the chirp is fitted by an iterative algorithm [8]. Then, the resulting amplitude of the fit curve (peak-to-valley) is plotted against the respective topography wavelength. If the amplitude deviates more than $\pm 50\%$ from the reference amplitude, the shortest wavelength of a measured sinusoidal structure which fulfills the transmission criterion is defined as small scale fidelity limit and thus, serves as discretized resolution parameter.

First, the excitation laser-focus (or point spread function, PSF) is used in its unmodified, initial state to fabricate the respective calibration structures with different excitation power values p . The lateral period length d and small scale fidelity limit ssf are plotted versus p (blue curves of Figure 4). Second, the aberrations of the excitation PSF are compensated with the help of a spatial light modulator and the method presented in Ref. [29]. Both material measures are fabricated again and the respective resolution limits are represented by the red curves of Figure 4. Third, the aforementioned second laser beam is introduced for STED-inspired DLW. Here, an aberration corrected [29] doughnut-mode is used to

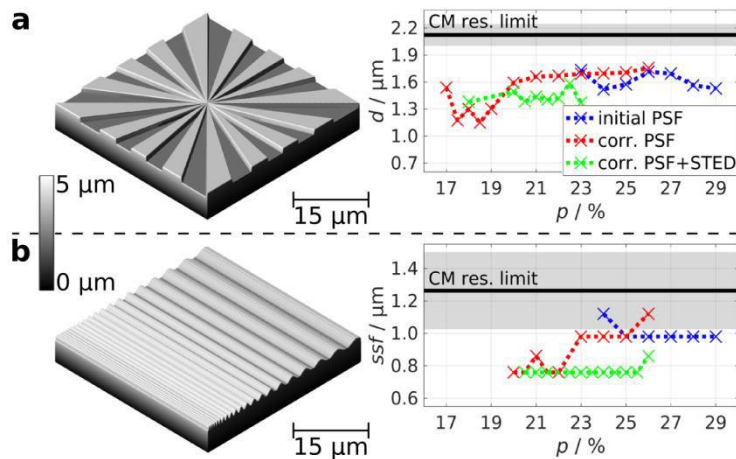


Figure 4. Lateral resolution of the DLW fabrication process. The lateral period limit d of the ASG-type measure (a) and the small scale fidelity limit ssf of the CIN-type measure (b) (CAD-data on the left-hand side) are investigated for different excitation power values p for the initial (blue) and the aberration corrected (red) excitation PSF. The additional presence of a depleting doughnut-mode is illustrated by the green curves. The highest resolved structures are used to determine the resolution limit of the confocal microscope with a 100x objective (black line with standard deviation in gray).

investigate its influence on the lateral resolution of the manufacturing process (green curves of Figure 4).

For both geometries it can be observed that the aberration correction procedure results in an improvement of the fabrication resolution. Without this correction, the excitation PSF is non-ideal shaped and enlarged in an inhomogeneous way, leading to a non-isotropic enlargement of the polymerization voxel. Therefore, unwanted side-effects (e.g. proximity) become more important and thus, result in a worsening of the resolution. Consequently, there is no clear dependence of the lateral period limit / small scale fidelity limit on the excitation power. In contrast, the resolution significantly improves with decreasing excitation power for the aberration corrected PSFs. Here, the laser-focus is not (or just barely) distorted. Thus, the above mentioned unwanted side-effects are much weaker. Moreover, aberration correction leads to a local compression of the incorporated intensity. As a result, the polymerization threshold shifts towards smaller excitation power values, allowing for fabricating with less power. These lower power values again lead to smaller (non-distorted) polymerization voxels, which improve the resolution as expected. For the ASG-type measure, the resolution value d at the lowest excitation power ($p = 17\%$) increases, because the polymerization threshold is not clearly exceeded, leading to a random proximity-induced polymerization. Of course, a lower resolution limit is the consequence.

Introducing the doughnut-mode for stimulated emission depletion obviously does not lead to a further improvement of the lateral resolution, but allows for a significant larger range of constant results instead. Especially for the CIN-type measure, the highest resolution can be kept over an excitation power range of 5%. This constant fabrication window reduces down to only 2% without the presence of the depleting mode and is more unstable. Thus, STED-inspired DLW allows for increasing the excitation power to enhance the structure's mechanical stability and reproducibility, while keeping the high resolution. Although the best lateral period limit d for the ASG-type measure decreases compared to the red curve, a more constant resolution limit over p can also be observed here. For higher excitation power values, this limit exceeds the resolution limit of the corrected PSF case and thus, confirms the results already found for the CIN-type measure. As reasons for the worse lateral period limit for low p -values, technical aspects have to be considered. Using the aforementioned software 'Describe', the structure is discretized into single layers, fabricated unidirectional by galvanometer deflections over the entire footprint. Therefore, only very small deflections occur within the center of the ASG-type measure, while the intensity of the excitation laser beam is ramped on and off very fast. As only the excitation laser beam can be controlled by the DLW software, the depleting laser is permanently focused into the center of the ASG-type structure, leading to an increased depletion of the polymerization and additional thermal influences. This might explain the worsening of the absolute lateral resolution limit d around the polymerization threshold.

In order to compare the resolution limits of the fabrication process with the resolution limits of the subsequent calibration procedure of the topography measuring instrument, the best resolved ASG-type and CIN-type measures are analyzed by the above mentioned confocal microscope with a 100x objective (black lines in Figure 4 with the respective standard deviations in gray). Since the resolution limits d and ssf are found to be about ($\sim 1-2$) μm (which is distinctly better than the industrial standard) and do not depend on the excitation power p , the geometries fabricated via DLW definitely fulfill any resolution requirements for the calibration of modern high-end industrial topography measuring instruments. In particular, the characteristics for the CIN-type measure are just good enough without the aberration compensation, whereas a corrected excitation PSF and the additional presence of a STED laser mode even exceed noticeably those resolution requirements and guarantee a sufficient structure quality and a large range of constant fabrication parameters. This is very reassuring, since the microscopic field is developing quickly. Therefore, corresponding calibration specimens are increasingly indispensable.

4. SUMMARY AND CONCLUSIONS

Regarding the increasing demand on easy and time-saving ISO-compliant calibration procedures, two-photon laser lithography appears to be the ideal fabrication method for the generation of multiple, application-specific calibration geometries on only one single sample. Development under UV exposure leads to constant calibration characteristics and thus, guarantees a very fast manufacturing of so-called 'universal-samples', suitable for the calibration of the most common characteristics. Further investigations of the fabrication method show that the realized manufacturing resolution strongly depends on the quality of the fabricating excitation laser-focus, which therefore allows for improving the structure's quality. A superposition with an additional doughnut-shaped laser-focus for stimulated emission depletion further improves the fabrication conditions. Higher excitation power values can be used to generate mechanically more stable

structures while keeping a high resolution. After all, the manufactured feature sizes distinctly exceed the general requirements for the industrial calibration of up-to-date optical topography measuring instruments. This provides potential for the quickly increasing and enhancing field of high resolution microscopy and adds to the application-scope of (STED-inspired) additive manufacturing.

5. ACKNOWLEDGEMENT

The authors gratefully acknowledge financial support from the Deutsche Forschungsgemeinschaft (DFG) within the Collaborative Research Center (SFB) 926 as well as the Nano Structuring Center (NSC) at the University of Kaiserslautern for the opportunity of sputtering processes and SEM sample analysis.

REFERENCES

- [1] Leach, R.K., [Characterisation of areal surface texture], Springer, Berlin & New York, 1-13 (2013).
- [2] Stout, K., [Development of methods for the characterisation of roughness in three dimensions], Penton Press, Rev. repr. London (2000).
- [3] Blunt, L., Jiang, X., [Advanced techniques for assessment surface topography: Development of a basis for 3D surface texture standards "SURFSTAND"], Kogan Page Science, London [u.a.] (2003).
- [4] ISO 25178-1, "Geometrical product specifications (GPS) - Surface texture: Areal - Part 1: Indication of surface texture" (2016).
- [5] Giusca, C.L., Leach, R.K., Helary, F., Gutauskas, T., Nimishakavi, L., "Calibration of the scales of areal surface topography-measuring instruments: part 1. Measurement noise and residual flatness," *Measurement Science and Technology* **23**(3), 035008 (2012).
- [6] Giusca, C.L., Leach, R.K., Helary, F., "Calibration of the scales of areal surface topography measuring instruments: part 2. Amplification, linearity and squareness," *Measurement Science and Technology* **23**(6), 065005 (2012).
- [7] Giusca, C.L., Leach, R.K., "Calibration of the scales of areal surface topography measuring instruments: part 3. Resolution," *Measurement Science and Technology* **24**(10), 105010 (2013).
- [8] Seewig, J., Eifler, M., Wiora, G., "Unambiguous evaluation of a chirp measurement standard," *Surf. Topogr.: Metrol. Prop.* **2**, 045003-045007 (2014).
- [9] Leach, R.K., Giusca, C.L., Rubert, P., "A single set of material measures for the calibration of areal surface topography measuring instruments: the NPL Areal Bento Box," *Proc. 14th MPES*, 406-413 (2013).
- [10] Maruo, S., Nakamura, O., Kawata, S., "Three-dimensional Microfabrication with two-photon-absorbed photopolymerization," *Opt. Lett.* **22**, 132-134 (1997).
- [11] Deubel, M., von Freymann, G., Wegener, M., Pereira, S., Busch, K., Soukoulis, C.M., "Direct laser writing of three-dimensional photonic-crystal templates for telecommunications," *Nature Materials* **3**(7), 444-447 (2004).
- [12] Hohmann, J.K., Renner, M., Waller, E.H., von Freymann, G., "Three-Dimensional μ -Printing: An Enabling Technology," *Adv. Optical Mater.* **3**, 1488-1507 (2015).
- [13] Van 't Oever, J., Spannenburg, N., Offerhaus, H., Van den Ende, D., Herek, J.L., Mugele, F., "In-chip direct laser writing of a centimeter-scale acoustic micromixer," *J. Micro Nanolithogr MEMS MOEMS* **14**(2), 023503 (2015).
- [14] Haske, W., Chen, V.W., Hales, J.M., Dong, W., Barlow, S., Marder, S.R., Perry, J.W., "65 nm feature sizes using visible wavelength 3-D multiphoton lithography," *Opt. Express*. **15**(6), 3426-3436 (2007).
- [15] Thiel, M., Fischer, J., von Freymann, G., Wegener, M., "Direct laser writing of three-dimensional submicron structures using a continuous-wave laser at 532 nm," *Appl.Phys.Lett.* **97**, 221102 (2010).
- [16] Deubel, M., von Freymann, G., Wegener, M., Pereira, S., Busch, K., Soukoulis, C.M., "Direct laser writing of three-dimensional photonic-crystal templates for telecommunications," *Nature Materials* **3**, 444-447 (2004).
- [17] Renner, M., von Freymann, G., "Spatial correlations and optical properties in three-dimensional deterministic aperiodic structures," *Scientific Reports* **5**, 13129 (2015).

- [18] Gissibl, T., Thiele, S., Herkommer, A., Giessen, H., "Two-photon direct laser writing of ultracompact multi-lens objectives," *Nature Photonics* **10**, 554-560 (2016).
- [19] Thiele, S., Arzenbacher, K., Gissibl, T., Giessen, H., Herkommer, A.M., "3D-printed eagle eye: Compound microlens system for foveated imaging," *Science Advances* **3**(2), e1602655 (2017).
- [20] Ceylan, H., Yasa, I.C., Sitti, M., "3D Chemical Patterning of Micromaterials for Encoded Functionality," *Adv.Mat.* **29**(9), 1605072 (2017).
- [21] Richter, B., Hahn, V., Bertels, S., Claus, T.K., Wegener, M., Delaittre, G., Barner-Kowollik, C., Bastmeyer, M., "Guiding Cell Attachment in 3D Microscaffolds Selectively Functionalized with Two Distinct Adhesion Proteins," *Adv.Mater.* **29**(5), 1604342 (2017).
- [22] Hohmann, J.K., von Freymann, G., "Influence of Direct Laser Written 3D Topographies on Proliferation and Differentiation of Osteoblast-like Cells: Towards improved implant surfaces," *Adv.Funct.Materials* **24**(42), 6573-6580 (2014).
- [23] Bückmann, T., Thiel, M., Kadic, M., Schittny, R., Wegener, M., "An elasto-mechanical unfeelability cloak made of pentamode metamaterials," *Nature Communications* **5**, 4130 (2014).
- [24] Bauer, J., Schroer, A., Schwaiger, R., Kraft, O., "Approaching theoretical strength in glassy carbon nanolattices," *Nature Materials* **15**, 438-443 (2016).
- [25] Eifler, M., Seewig, J., Hering, J., von Freymann, G., "Calibration of z-axis linearity for arbitrary optical topography measuring instruments," *Proc. SPIE 9525: Optical Measurement Systems for Industrial Inspection IX*, 952510 (2015).
- [26] Ströer, F., Hering, J., Eifler, M., Raid, I., von Freymann, G., Seewig, J., "Ultrafast 3D High Precision Print of Micro Structures for Optical Instrument Calibration Procedures," *Additive Manufacturing* **18**, 22-30 (2017).
- [27] Eifler, M., Hering, J., von Freymann, G., Seewig, J., "Manufacturing of the ISO 25178-70 material measures with direct laser writing – a feasibility study," *Met&Props* (submitted).
- [28] Waller, E.H., Renner, M., von Freymann, G., "Active aberration- and point-spread-function control in direct laser writing," *Opt. Express* **20**(22), 24949–24956 (2012).
- [29] Hering, J., Waller, E.H., von Freymann, G., "Automated aberration correction of arbitrary laser modes in high numerical aperture systems," *Opt. Express* **24**(25), 28500-28505 (2016).
- [30] Jesacher, A., Booth, M.J., "Parallel direct laser writing in three dimensions with spatially dependent aberration correction," *Opt. Express* **18**(20), 21090-21099 (2010).
- [31] Waller, E.H., von Freymann, G., "Multi foci with diffraction limited resolution," *Opt. Express* **21**(18), 21708-21713 (2013).
- [32] Abbe, E., "Beiträge zur Theorie des Mikroskops und der mikroskopischen Wahrnehmung," *Archiv für mikroskopische Anatomie* **9**(1), 413-468 (1873).
- [33] Hell, S.W., Wichmann, J., "Breaking the diffraction resolution limit by stimulated emission: stimulated-emission-depletion fluorescence microscopy," *Optics Letters* **19**(11), 780-782 (1994).
- [34] Klar, T., Hell, S.W., "Subdiffraction resolution in far-field fluorescence microscopy," *Optics Letters* **24**(14), 954-956 (1999).
- [35] Fischer, J., Wegener, M., "Three-dimensional optical laser lithography beyond the diffraction limit," *Laser Photonics Rev.* **7**(1), 22–44 (2013).
- [36] Wollhofen, R., Katzmann, J., Hrelescu, C., Jacak, J., Klar, T.A., "120 nm resolution and 55 nm structure size in STED-lithography," *Opt. Express* **21**(9), 10831-10840 (2013).
- [37] Oakdale, J.S., Ye, J., Smith, W.L., Biener, J., "Post-print UV curing method for improving the mechanical properties of prototypes derived from two-photon lithography," *Opt. Express* **24**(24), 27077-27086 (2016).
- [38] Polyanskiy, M.N., "Refractive index database," <https://refractiveindex.info> (10 November 2017).
- [39] Samsonov, G.V., [Handbook of the Physicochemical Properties of the Elements], Springer, Boston, MA, 387-446 (1968).
- [40] PGM Database, <http://pgmdatabase.com> (10 November 2017).
- [41] DIN 50035, "Terms and definitions used on ageing of materials – Polymeric materials" (2012).
- [42] Klauer, K., Eifler, M., Schneider, F., Seewig, J., Aurich, J.C., "Ageing of roughness artefacts – impact on the measurement results," *Proc. of euspen's 17th Int. Conf. & Exhibition*, Hannover, 403-404 (2017).
- [43] Krüger-Sehm, R., Bakucz, P., Jung, L., Wilhelms, H., "Chirp-Kalibriernormale für Oberflächenmessgeräte (Chirp Calibration Standards for Surface Measuring Instruments)," *tm - Technisches Messen* **74**(11), 572-576 (2007).